CrossMark

ORIGINAL PAPER

A subsidiary fast-diffusing substitution mechanism of Al in forsterite investigated using diffusion experiments under controlled thermodynamic conditions

Irina Zhukova[1] · **Hugh O'Neill**[1] · **Ian H. Campbell**[1]

Abstract Diffusion of Al in synthetic forsterite was studied at atmospheric pressure from 1100 to 1500 °C in air along [100] with activities of SiO_2, MgO and Al_2O_3 (a_{SiO2}, a_{MgO} and a_{Al2O3}) buffered. At low a_{SiO2}, the buffer was forsterite + spinel + periclase (fo + sp + per) at all temperatures, while at high a_{SiO2} and subsolidus conditions a variety of three-phase assemblages containing forsterite and two other phases from spinel, cordierite, protoenstatite or sapphirine were used at 1100–1350 °C. Experiments at high a_{SiO2} and 1400 °C used forsterite + protoenstatite + melt (fo + en + melt), and at 1500 °C, fo + melt. The resulting diffusion profiles were analysed by LA–ICP–MS in scanning mode. Diffusion profiles in the high a_{SiO2} experiments were generally several hundred microns in length, but diffusion at low a_{SiO2} was three orders of magnitude slower than in high a_{SiO2} experiments carried out at the same temperature, producing short profiles only a few microns in length and close to the spatial resolution of the analytical method. Interface concentrations of Al in the forsterite, obtained by extrapolating the diffusion profiles to the crystal/buffer interface, were only a fraction of those expected at equilibrium, and varied among the differing buffer assemblages according to $(a_{Al2O3})^{1/2}$ and $(a_{SiO2})^{3/4}$, pointing to the substitution of Al in forsterite by an octahedral-site, vacancy-coupled (OSVC) component with the stoichiometry $Al_{4/3}^{3+}vac_{2/3}SiO_4$, whereas the main substitution expected from previous equilibrium studies would be the coupled substitution of 2 Al for Mg + Si, giving the stoichiometry $MgAl_2O_4$. It is proposed that this latter substitution is not seen on the length scales of the present experiments because it requires replacement of Si by Al on tetrahedral sites, and is accordingly rate-limited by the slow diffusivity of Si. Instead, diffusion of Al by the OSVC mechanism is relatively fast, and at high a_{SiO2}, even faster than Fe–Mg interdiffusion.

Introduction

Although it is a major element in basaltic systems, aluminium substitutes into olivine only at trace-element concentrations, typically at 0.1 wt% or less. Nevertheless such small amounts can now be determined with enough precision to be petrologically informative, whether by electron microprobe (e.g., Batanova et al. 2015) or laser-ablation ICP–MS (e.g., Foley et al. 2011). The solubility of Al in olivine coexisting with spinel has been calibrated as a geothermometer (Wan et al. 2008; Coogan et al. 2014), and has been applied to determine the liquidus temperatures of mafic and ultramafic magmas from olivine phenocrysts that have spinel inclusions (e.g., Coogan et al. 2014; Spice et al. 2015; Heinonen et al. 2015). Part of the usefulness of Al-in-olivine geothermometry stems from the apparently low diffusivity of Al in olivine (Spandler et al. 2007; Spandler and O'Neill 2010), which is advantageous in preserving Al contents at the time of crystallization against subsequent reequilibration, as also found for P (see, for example, Batanova et al. 2015, their Fig. 1). Mantle olivines may also retain an
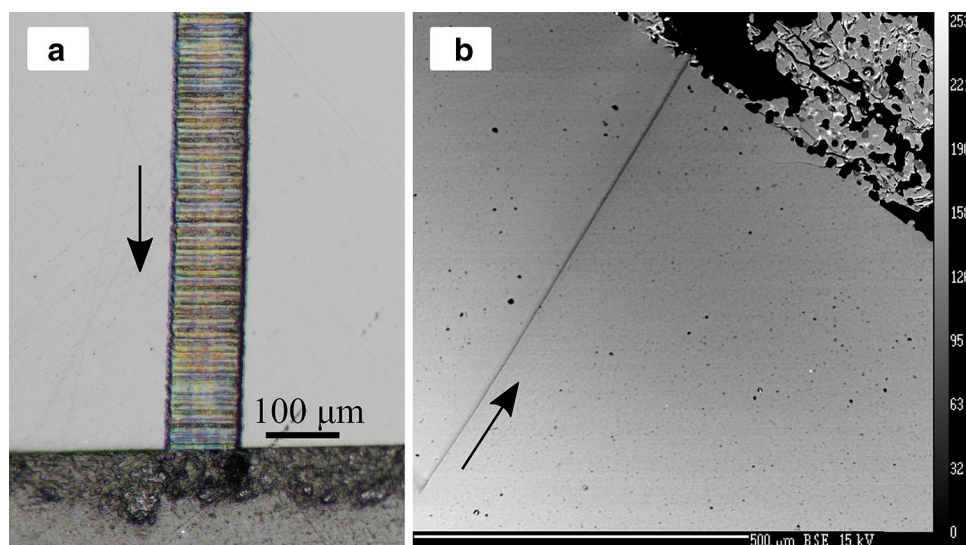
Fig. 1 a Microphoto of a typical laser-ablation inductively-coupled-plasma mass spectrometry (LA–ICP–MS) traverses, showing the source layer, forsterite crystal and the spatial relationship between the laser ablation trace and the diffusion interface after analysis. Experiment with pre-annealing run at 1300°, in air for 240 h. **b** Back scatter electron (BSE) image of a San Carlos olivine and source layer after quenching and analysis. The experiment was run at 1300°, log$f$O$_2$ = −5.8 for 312 h. The line of the laser trace is faint in the BSE image because the crystal was repolished before carbon coating. The *arrow* next to the laser trace indicates the direction of the beam scan
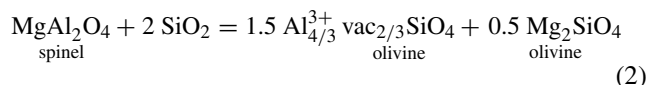
inhomogeneous distribution of Al and P where the majority of other trace elements have been homogenized by diffusion (Mallmann et al. 2009; McKibbin et al. 2013).

The apparently slow diffusivity of Al in olivine is explicable if its mobility is controlled by its substitution onto the tetrahedral cation sites of the olivine crystal structure. Si, the main occupant of these tetrahedral sites, is known to diffuse more slowly by several orders of magnitude than the octahedrally coordinated major-element cations, Mg and Fe, in olivine (Chakraborty 2010). The slow diffusivity of P has likewise been attributed to its tetrahedral site occupancy (Milman-Barris et al. 2008; Mallmann et al. 2009; McKibbin et al. 2013; Watson et al. 2015). In forsteritic olivine (i.e., near-end-member Mg$_2$SiO$_4$) in the system CaO–MgO–Al$_2$O$_3$–SiO$_2$ (CMAS) at liquidus temperatures (1400 °C), Al substitutes into olivine by the coupled substitution of 2 Al^{3+} for Mg^{2+} + Si^{4+}, with half the Al^{3+} substituting for Mg^{2+} on an octahedral site charge-balanced by the other half substituting for Si^{4+} on an adjacent tetrahedral site (Evans et al. 2008). The change in the olivine/melt partition coefficient of Al with its concentration reflects a high degree of short-range order between the octahedral and tetrahedral Al (Evans et al. 2008). If this short-range order is conserved during Al diffusion, then both the octahedral and tetrahedral Al concentrations would be rate-limited by the removal of Si to make way for Al on the tetrahedral sites. We would then expect the diffusivity of Al to be similar to that of Si.

There is independent evidence that the substitution of Al in olivine predominantly occurs by this mechanism, for which the governing equilibrium may be written:

$$\underset{\text{spinel}}{MgAl_2O_4} = \underset{\text{olivine}}{MgAl_2O_4} \tag{1}$$

This mechanism (2 Al^{3+} for Mg^{2+} + Si^{4+}) is independent of the activity of silica (a$_{SiO2}$), which was used by Coogan et al. (2014) to show experimentally that it is likely to be the dominant one. It contrasts with the mechanism proposed for larger 3+ cations such as Sc^{3+} and REE^{3+} that are restricted to octahedral sites. In these cases, charge-balance is achieved by octahedral site vacancies, giving the stoichiometry R$_{4/3}$$^{3+}vac_{2/3}SiO_4$, where vac stands for a cation vacancy on an octahedral site (Evans et al. 2008). The governing equilibrium for this mechanism is:

$$\underset{\text{spinel}}{MgAl_2O_4} + 2\ SiO_2 = 1.5\ \underset{\text{olivine}}{Al_{4/3}^{3+}vac_{2/3}SiO_4} + 0.5\ \underset{\text{olivine}}{Mg_2SiO_4} \tag{2}$$

The mobility of 3+ cations substituting by this mechanism would not be limited by tetrahedral site mobility, and indeed it is found that the rates of diffusion of the larger R^{3+} cations are similar to those of other octahedrally coordinated cations in olivine, whether these are 2+ or 4+ (Spandler et al. 2007; Spandler and O'Neill 2010, Qian et al. 2010; Tollan et al. 2015; Jollands et al. 2016b).

There is no theoretical reason for the substitution of an impurity in a crystal to occur just by one mechanism only.

Indeed, it has been shown by infra-red spectroscopy that $-H^+$ commonly substitutes in olivine to form OH^- anions by four different mechanisms (e.g., Berry et al. 2005), with yet more mechanisms in other, less common chemical environments (e.g., Ingrin et al. 2014). Although Coogan et al. (2014) showed that most of the Al in olivine is by the coupled substitution of reaction (1), they did not exclude the possibility that some proportion of the Al in olivine might be substituting by the alternative mechanism of reaction (2). That this may be the case occurred to us during an investigation of Ni and Co diffusion in synthetic forsterite (Zhukova et al., 2014), when we observed that small amounts of Al appeared to be diffusing on relatively fast time scales either out of the forsterite, starting from the indigenous impurity content of ~30 ppm (Table 1 in Zhukova et al. 2014), or into the olivine from external contamination when experiments were run at high temperature in alumina muffle tubes.

We have therefore undertaken an experimental campaign to study the solubility and diffusivity of the Al in forsterite that substitutes by the fast-diffusion mechanism, by exploiting this fast diffusion property. Our experimental approach was to diffuse Al into single crystals of forsterite, using three-phase buffer assemblages in the system $MgO–Al_2O_3–SiO_2$ as the source, for durations that would not be expected to produce diffusion profiles measurable on the ~5 μm length scale of our analytical method, given the rates of tetrahedral-site diffusion implied by Si diffusion measurements (e.g., Fei et al. 2012). Where three crystalline phases are present, the activities of the three relevant components MgO, Al_2O_3 and SiO_2 are fully specified at a given temperature and pressure (here, atmospheric pressure). Activities are also fixed in those experiments where melt is present, by the composition of the melt. The solubility

of Al associated with the fast-diffusion mechanism is then obtained from fitting the observed concentration profiles to the usual one-dimensional diffusion equation, which gives the crystal/buffer interface concentrations. These concentrations may then be compared to the concentrations in equilibrium with spinel obtained in the experiments by Wan et al. (2008) and Coogan et al. (2014), which, insofar as they form the basis of the geothermometer, have been robustly tested against Al concentrations in natural olivines. Moreover, the stoichiometry of the fast-diffusion substitution mechanism can be inferred from the variation of the interface solubilities with the activities imposed by the different three-phase buffer assemblages. At the same time, the rates of Al diffusion according to its fast-diffusion mechanism are quantified. We also present results from the same approach applied to natural San Carlos olivine. To our knowledge, this is the first systematic, quantitative investigation of the thermodynamics of a kinetically constrained impurity substitution into a geologically important mineral.

Experimental technique

The diffusion experiments were performed as previously described in Zhukova et al. (2014), Jollands al at. (2014, 2016a, b). Starting materials were synthetic forsterite and San Carlos olivine (sco). A high purity single crystal of synthetic forsterite, grown by the Czochralski method (Martrosov et al. 2002), was obtained from Solix Ltd. Minsk, Belarus (http://www.solix-crystal.com). The Fe content of the crystal was less than 1.5 ppm and the Al_2O_3 concentration 30 ppm. The concentration of Al_2O_3 in the San Carlos olivine was 200 ppm. The forsterite crystal was cut (0.3 × 0.3 × 0.3 cm) and polished perpendicular to [100] axis. The San Carlos olivine crystal was cut and polished as dictated by its shape. The planes were polished using SiC paper (p 800–1200), then by 6- and 3 μm diamond paste on a ceramic or tin lap, and finally 0.2 μm silica paste on a vibration polishing machine to eliminate remaining surface defects.

The activities of SiO_2, MgO and Al_2O_3 were buffered in each experiment by three-phase assemblages at subsolidus temperatures (<1350 °C, see Mao et al. 2005), or by forsterite plus silicate melt, as listed in Table 1 and described below. For the San Carlos olivine experiments, the buffering assemblages were made with molar FeO/(FeO + MgO) = 0.1. Buffer powders were made from oxide mixes ground in an agate mortar, pressed to form a pellets and then heated in a box furnace for 1 day at the temperature of the experiment. These pellets were crushed again, mixed into a slurry with polyethylene oxide, and painted on to the polished face of the crystals. The assembly was then dried in an oven at 110 °C.

Table 1 Composition of buffer assemblages (wt%)

Mineral assemblage	SiO₂	MgO	Al₂O₃	FeO	sco
Experiments with forsterite					
fo + sp + per	11.45	69.13	19.43		
fo + spr + sp	14.26	32.52	53.22		
fo + crd + sp (fo + crd + spr)*	35.31	30.46	34.24		
fo + en + crd	51.71	38.54	9.75		
Experiments with San Carlos olivine at 1300 °C					
sco + crd + sp	1.93	3.50	11.55	0.34	82.68

Minerals: *fo* forsterite (Mg_2SiO_4), *en* enstatite ($MgSiO_3$), *per* periclase (MgO), *sp* spinel ($MgAl_2O_4$), *spr* sapphirine ($Mg_4A_{18}Si_2O_{20}$), *crd* cordierite ($Mg_2Al_4Si_5O_{18}$), *sco* San Carlos olivine ($Mg_{1.8}Fe_{0.2}SiO_4$), *mw* magnesiowüstite ($Mg_{0.9}Fe_{0.1}O$), *opx* orthopyroxene ($Mg_{1.8}Fe_{0.2}Si_2O_6$)

* fo + crd + sp in experiments at 1250–1500 °C and fo + crd + spr in experiments at 1100–1250 °C (see text for details)

Diffusion experiments were performed in one-atmosphere vertical tube furnaces modified to control the fO_2 by CO–CO$_2$ gas mixing, or in a box furnace in air. In the vertical tube furnace, the crystals plus their adhering buffer mixes were suspended by platinum wire in a "chandelier", whereas in the box furnace they were placed in alumina crucibles. Experiments were run for 10–28 days at temperatures from 1100 to 1500 °C and logfO_2 from −0.7 to −5.8. The experiment with the San Carlos olivine was performed at 1300 °C and at logfO_2 = −5.8.

The diffusion and possibly the solubility of allovalent impurity species charge-balanced by vacancies or interstitials in crystals may depend on the point-defect concentration. One possible complication is that the point-defect concentration in the Czochralski-grown crystal does not reach the equilibrium imposed by the three-phase buffer. In order to test for this possibility, we performed some experiments after pre-annealing the forsterite crystals. These experiments were run in two stages. For the first stage, crystals were annealed in equilibrium with Al-free buffers with high (fo + per) and low (fo + en) silica activities. Forsterite crystals with buffer powders painted on their polished side were annealed at 1300 °C in a box furnace in the air for 2 days. The buffer powders were then removed by immersion in a solution of citranox in an ultrasonic bath. In the second stage, the crystals were covered with buffer assemblages (fo + sp + per, fo + crd + sp or fo + en + crd) that contained Al, and experiments were run as normal at 1300 °C for 10 days. Details of the experimental conditions are summarized in Table 4.

Analytical methods

Concentration profiles were analysed by LA-ICP-MS using an Agilent 7500S quadrupole ICP-MS coupled to a Conpex 110 nm excimer laser with a custom-built, fast-washout ablation chamber. The analyses were carried out using the traversing technique of Spandler and O'Neill (2010) with a pulse rate of 5 Hz, and energy output from the laser of about 50 mJ. The laser beam, focused by a rectangular slit (100 × 5 μm), was traversed perpendicular to the polished surface starting from lower concentrations toward the interface at a rate of 1 or 8 μm/s (Fig. 1). Background was counted for 30 s before every measurement. Calibration was performed using the standard reference materials: NIST 612, 610, with ^{29}Si as the internal standard. The Si content of forsterite and sco had been previously measured by SEM and ^{29}Si calculated assuming the natural isotope ratio. Detection limits for ^{27}Al are a few parts per billion, orders of magnitude lower than the levels of Al concentrations that need to be determined in this study. The concentrations of Al in forsterite or San Carlos olivine have not been corrected for matrix effects,
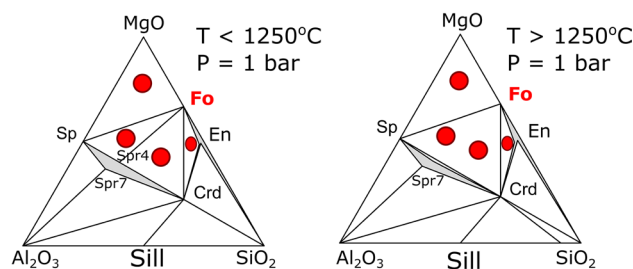

Fig. 2 Mineral parageneses in the system SiO$_2$–MgO–Al$_2$O$_3$. *Fo* forsterite Mg$_2$SiO$_4$; *Sp* spinel, MgAl$_2$O$_4$; *En* enstatite, MgSiO$_3$; *Spr4* sapphirine, Mg$_4$Al$_8$Si$_2$O$_{20}$, *Spr7* Mg$_{3.5}$Al$_9$Si$_{1.5}$O$_{20}$; *Crd* cordierite, Mg$_2$Al$_4$Si$_5$O$_{18}$. *Large dots* show buffer compositions used for experiments. *Grey fields* represent associations with solid solutions in enstatite and sapphirine

which may be significant: for other elements in olivine, correction factors as large as 20% have been indicated by comparison to values determined by electron microprobe analysis (see Tuff and O'Neill 2010, their Table 6). This should be kept in mind in comparing results with literature data (Fig. 2).

The position of the interface was determined from the abrupt change in slope of the ^{29}Si profiles, together with a sharp rise of doped element concentrations. The uncertainty in the position of the interface is 3–5 μm.

Activities of SiO$_2$, MgO and Al$_2$O$_3$

For the experiments with forsterite, the activities of all three components in the system MgO–Al$_2$O$_3$–SiO$_2$ were defined by the three-phase assemblages at temperatures below 1350 °C shown in Fig. 2. This diagram was calculated at 1 bar pressure from the thermodynamic data in Holland and Powell (2011) using the PerpleX 6.5 package (Connolly and Petrini, 2002). At 1100 and 1200 °C there are four three-phase assemblages containing forsterite, involving the phases spinel (sp), sapphirine (spr), cordierite (crd) and protoenstatite (en): (1) fo + sp + per, (2) fo + spr + sp, (3) fo + spr + crd, and (4) fo + crd + en. The stability field of sapphirine (Spr4, with ideal formula Mg$_4$Al$_8$Si$_2$O$_{20}$) in equilibrium with fo terminates near 1250 °C through the reaction fo + spr = sp + cd, so at 1300 °C there are three three-phase assemblages, fo + sp + per, fo + sp + crd and fo + crd + en. At 1400 and 1500 °C, the assemblage fo + sp + per remains subsolidus, but the other assemblages melt to produce fo + en + melt and fo + melt, respectively (Mao et al. 2005). The changes in the activities of SiO$_2$, MgO and Al$_2$O$_3$ (a_{SiO2}, a_{Al2O3}, a_{MgO}) in these melt-containing assemblages, relative to the hypothetical equivalent unstable subsolidus assemblages, are relatively minor, and thus for the purposes of this study we calculate values of a_{SiO2}, a_{Al2O3}, a_{MgO} in the fo + en + melt and

Table 2 Activities of SiO_2, MgO and Al_2O_3 calculated for the solid mineral assemblages used in the experiments, calculated from the thermodynamic data of Holland and Powell (2011)

	a	b
fo + per + sp $T = 1100–1500$ C		
SiO_2	2.15	−6857.7
MgO	1.00	0
Al_2O_3	−1.33	−2082.4
fo + sp + crd $T > 1250$ C		
SiO_2	−0.53	−439.8
MgO	0.04	−2959.3
Al_2O_3	−1.40	927.4
fo + en + crd $T = 1100–1500$ C		
SiO_2	−0.70	247.1
MgO	0.10	−3253.6
Al_2O_3	−1.14	−277.7

$\ln a_{SiO_2} = a + b/T$, $\ln a_{MgO} = a + b/T$, $\ln a_{Al_2O_3} = a + b/T$

fo + melt assemblages from the thermodynamic data for the unstable subsolidus assemblages corresponding to the buffer starting composition. For convenience, these activities are given parameterized as a function of temperature in Table 2, using a standard state of 1 bar and the temperature of interest, relative to the pure phases quartz (SiO_2), MgO (periclase), and Al_2O_3 (corundum). Note that as all assemblages contain forsterite (except the experiment on the San Carlos olivine), the quotient $a_{SiO_2} \cdot (a_{MgO})^2$ is constant in all assemblages at a given temperature, subsolidus or otherwise. The equations used for the calculations of activities are summarised in Table 3.

The activity of silica (a_{SiO_2}) calculated for these assemblages is shown as a function of temperature in Fig. 3. In the three-phase assemblage per + sp + fo, a_{SiO_2} increases with temperature, whereas for the fo + crd + en buffer there

is almost no temperature dependence. Activities of SiO_2 in fo + crd + sp and fo + en + crd assemblages are similar, between 0.45 and 0.58, whereas a_{SiO_2} in fo + sp + per assemblage is significantly lower at 0.11–0.18 (Table 2; Fig. 3). The assemblage fo + sp + per will hereafter be designated as having "low a_{SiO_2}" while those buffered by the other three-phase assemblages or melt-containing assemblages will all be described as having "high a_{SiO_2}".

Results

Long diffusion profiles (100–2500 μm) were obtained in the experiments at high a_{SiO2}, whereas at low a_{SiO2} profiles were generally only a few 10 s of microns (see Fig. 4). The long profiles had good error-function shapes, except, in many cases, for a sharp increase in Al concentration within a short distance of the interface (a few microns), which may be due to either contamination from the three-phase buffer source material at the interface, or from enhanced Al solubility by a second, much slower diffusion mechanism. The spatial resolution of our analytical technique is not sufficient to resolve the difference. Note that if the rate of tetrahedral-site diffusion is similar to that of Si diffusion measured by Fei et al. (2012), which is $10^{-18.6}$ m^2 s^{-1} at 1500 °C, the implied diffusion length scale of ~$Dt^{1/2}$ would be only 0.6 μm after 15 days, well below the resolution of our analytical method. Si diffusivities reported by Jaoul et al. (1983) are two orders of magnitude slower. The short profiles from the low a_{SiO2} experiments were too poorly resolved to check their shapes with any certainty, and for these the error function shape should be acknowledged to be an assumption rather than an observation (Table 3).

The shortness of these profiles relative to our analytical scale also means that the uncertainty in the location of the interface (3–5 μm) propagates into larger uncertainties on

Table 3 Reactions used for calculation of major-element component activities

Mineral association	Activity	Reaction	$\ln K=$
fo + sp + per	SiO_2	$2MgO(per) + SiO_2(qtz) = Mg_2SiO_4(fo)$	$-\ln(a_{SiO_2})$
	MgO	$/a_{MgO} = 1/$	
	Al_2O_3	$MgO(per) + Al_2O_3(cor) = MgAl_2O_4(sp)$	$-\ln(a_{Al_2O_3})$
fo + crd + sp	SiO_2	$2MgAl_2O_4(sp) + 5SiO_2(qtz) = Mg_2Al_4Si_5O_{18}(crd)$	$-5 \times \ln(a_{SiO_2})$
	MgO	$10MgO(per) + Mg_2Al_4Si_5O_{18}(crd) = 2MgAl_2O_4(sp) + 5Mg_2SiO_4(fo)$	$-10 \times \ln(a_{MgO})$
	Al_2O_3	$10Al_2O_3 + 5Mg_2SiO_4(fo) = Mg_2Al_4Si_5O_{18}(crd) + 8MgAl_2O_4(sp)$	$-10 \times \ln(a_{Al_2O_3})$
fo + en + crd	SiO_2	$Mg_2SiO_4(fo) + SiO_2(qtz) = Mg_2Si_2O_6(en)$	$-\ln(a_{SiO_2})$
	MgO	$Mg_2Si_2O_6(en) + 2MgO(per) = 2Mg_2SiO_4(fo)$	$-2 \times \ln(a_{MgO})$
	Al_2O_3	$4Mg_2Si_2O_6(en) + 2Al_2O_3 = 3Mg_2SiO_4(fo) + Mg_2Al_4Si_5O_{18}(crd)$	$-2 \times \ln(a_{Al2O3})$

Fig. 3 Phase diagram SiO_2–MgO–Al_2O_3 calculated at 1 *bar* and $Al_2O_3/(MgO + Al_2O_3) = 0.2$. *Dashed lines* indicate superliquidus conditions where the assemblages are unstable with respect to melt (Mao et al. 2005)

the interface concentrations and diffusion coefficients of these experiments, as discussed in Zhukova et al. (2014).

The error-function part of the concentration profiles were fitted by nonlinear least squares to the solution to Fick's equations for one-dimensional diffusion in a semi-infinite medium with the source reservoir maintained at constant concentration:

$$C(x) = C_i + (C_0 - C_i)\mathrm{erf}\left(x/2(Dt)^{1/2}\right) \tag{3}$$

where x is the distance from the interface, C_i is the interface concentration (here, the interface concentration for the fast-diffusion substitution mechanism producing the error-function-shaped profile), C_0 is the initial concentration as seen in the interior of the crystal, D is the diffusion coefficient and t is time. Values of $(Dt)^{1/2}$, C_i and C_0 were obtained for each profile. The fits of the profiles to Eq. 3 were generally excellent, with deviations to all diffusion profiles lying within the range of 6–10%. Some examples of the fits are shown in Fig. 4. The quoted uncertainties were derived from the averages obtained for individual profiles.

The results are summarised in Table 4. Experiments repeated for different durations (i.e. 1300 °C for 13, 25 and 28 days and 1400 °C for 10 and 14 days) gave similar results. Most experiments were run in air, but one experiment at lower fO_2 (log $fO_2 = -5.8$ at 1300 °C) produced no resolvable difference, nor did pre-annealing: diffusion

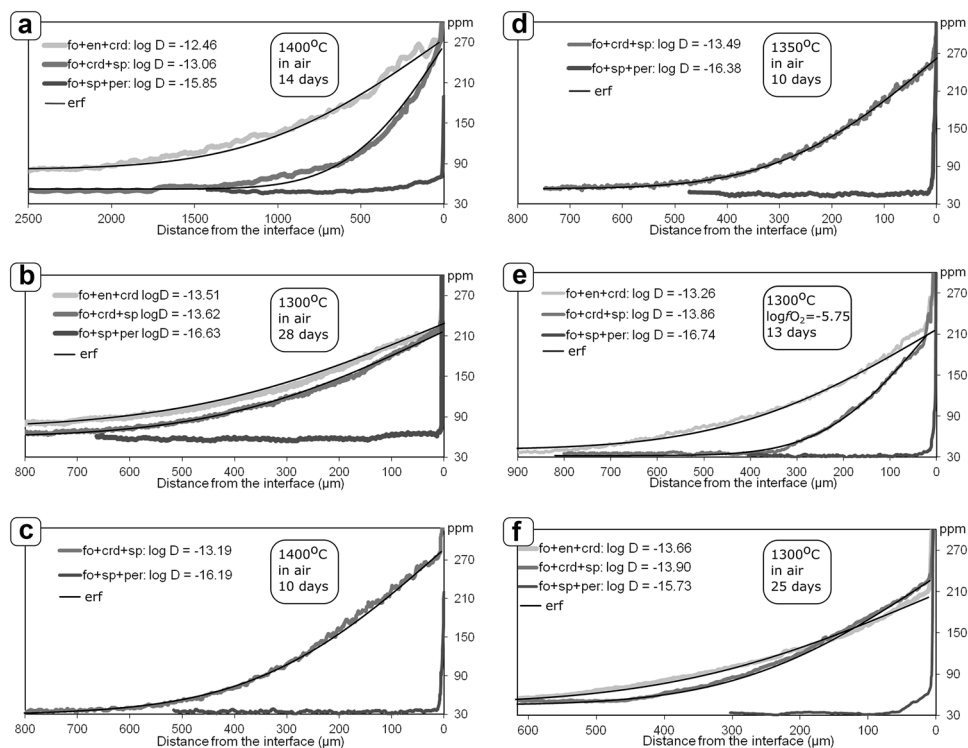**Fig. 4** Diffusion profiles of Al in forsterite measured by LA-ICP-MS

Table 4 Diffusion coefficients (m²/s) and concentrations of Al_2O_3 and Zn in olivine

T, °C	Duration (h)	Buffer	logfO_2	QFM+	log D (m²/s)	σ	Al_2O_3 (ppm)	σ
Diffusion Al in forsterite								
1500	360	fo + sp + per	−0.68	4.82	−15.51	0.48	80	8
1500	360	fo + en + crd	−0.68	4.82	−11.92	0.35	450	15
1400	336	fo + sp + per	−0.68	5.64	−15.85	0.2	75	9
1400	336	fo + crd + sp	−0.68	5.64	−13.06	0.05	270	14
1400	336	fo+en+crd	−0.68	5.64	−12.46	0.05	270	13
1400	240	fo + sp + per	−0.68	5.64	−16.19	0.09	68	7
1400	240	fo + crd + sp	−0.68	5.64	−13.19	0.07	300	15
1350	240	fo + sp + per	−0.68	6.09	−16.38	0.09	76	9
1350	240	fo + en + crd	−0.68	6.09	−13.49	0.07	260	12
1300	312	fo + sp + per	−5.8	1.54	−16.74	0.08	115	13
1300	312	fo + crd + sp	−5.8	1.54	−13.86	0.06	220	11
1300	312	fo + en + crd	−5.8	1.54	−13.26	0.07	220	11
1300	600	fo + sp + per	−0.68	6.57	−15.73	0.09	70	6
1300	600	fo + crd + sp	−0.68	6.57	−13.90	0.07	230	11
1300	600	fo + en + crd	−0.68	6.57	−13.66	0.06	202	11
1300	672	fo + sp + per	−0.68	6.57	−16.63	0.07	70	7
1300	672	fo + crd + sp	−0.68	6.57	−13.62	0.06	215	9
1300	672	fo + en + crd	−0.68	6.57	−13.51	0.06	215	9
1200	240	fo + sp + per	−0.68	7.62	−17.25	0.09	50	6
1200	240	fo + en + crd	−0.68	7.62	−14.08	0.06	145	10
1100	600	fo + sp + per	−0.68	8.83	≤18.75	0.49	45	7
1100	600	fo + spr + sp	−0.68	8.83	−16.04	0.49	130	9
1100	600	fo + crd + spr	−0.68	8.83	−15.73	0.43	180	11
Diffusion Al in forsterite with pre-annealing								
1300	240	fo + sp + per	−0.68	6.6	−16.10	0.18	44	2
1300	240	fo + crd + sp	−0.68	6.6	−13.53	0.15	215	35
1300	240	fo + en + crd	−0.68	6.6	−13.21	0.11	220	21
Diffusion Al in San Carlos olivine								
1300	312	sco + crd + sp	−5.8	1.5	−14.72	0.14	430	50

T, °C	h	Buffer	logfO_2	QFM+	log D (m²/s)	σ	Zn (ppm)	σ
Diffusion Zn out in San Carlos olivine								
1300	312	sco + mgwu + sp	−5.8	1.5	−13.98	0.12	57.4	3.3
1300	312	sco + crd + sp	−5.8	1.5	−13.93	0.12	54	2.8
1300	312	sco + opx + crd	−5.8	1.5	−13.97	0.12	51.2	2

Diffusion coefficient and concentrations are the average values for 1–5 parallel profiles measured by LA–ICP–MS

coefficients and the solubility of Al at the interface remain the same within the experimental uncertainty.

The concentrations of Al in forsterite at the crystal/buffer interfaces obtained in our experiments increased as a function of temperature for each buffer assemblage (Fig. 5a), but are very much less than those found in equilibrium experiments, as summarized in Table 5. These equilibrium solubilities are considered robust because of the realistic results obtained for the Al-in-olivine geothermometers (e.g. Coogan et al. 2014). The interface solubilites from the assemblages containing $MgAl_2O_4$ spinel,

namely fo + crd + sp (high a_{SIO_2}) and fo + sp + per (low a_{SIO_2}) differ considerably, being about three times lower in the low a_{SiO_2} experiments. This stands in contrast to the results of Coogan et al. (2014), who showed that the equilibrium Al solubility was more-or-less insensitive to a_{SIO_2}

This difference in solubilities with buffering assemblages provides quantitative evidence in support of the hypothesis that the diffusing Al is substituting by the octahedral-site, vacancy-coupled (OSVC) mechanism, with stoichiometry $Al^{3+}_{4/3}vac_{2/3}SiO_4$. The reaction governing this substitution may be written:

Fig. 5 **a** Concentrations of Al_2O_3 in forsterite as a function of inverse temperature for two different buffer assemblages. The solubility of Al_2O_3 in olivine is less than that found in equilibrium experiments (Wan et al. 2008). Note that there is melt present in experiments at 1400 and 1500 °C. **b** Logarithm of the equilibrium constant ($K*$) of the reaction: ¾ SiO_2 + ½ Al_2O_3 = ¾ $Al_{4/3}^{3+}vac_{2/3}SiO_4$ calculated as a function of inverse temperature for the three different buffer assemblages
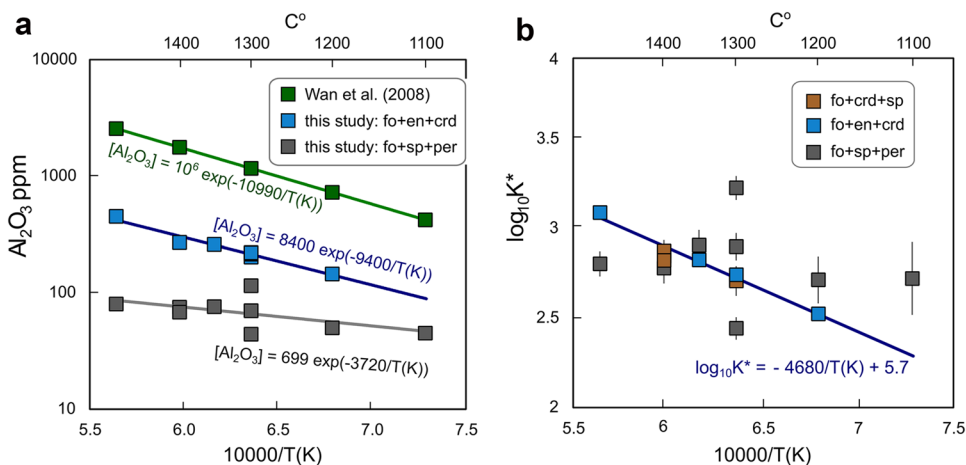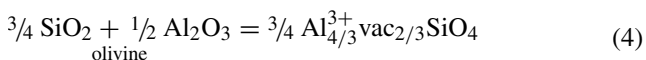
Table 5 Concentrations of Al_2O_3 in forsterite in equilibrium with $MgAl_2O_4$ spinel from equilibrium studies

Al_2O_3 in olivine (ppm)	X_{Mg}	Oxygen fugacity	T (°C)	References
1163	0.91	QFM −1.5, −1.8	1300	Wan et al. (2008)
755 ± 25	0.88	~QFM	1300	Agee and Walker (1990)
1585 ± 104	100	QFM+ 5.6 (in air)	1400	Evans et al. (2008)
822 (calculated from $D_{Al}Ol/melt$)	100	~QFM	1400	Beattie (1994)

$$\tfrac{3}{4}\ SiO_2 + \tfrac{1}{2}\ Al_2O_3 = \tfrac{3}{4}\ Al_{4/3}^{3+}vac_{2/3}SiO_4 \underset{olivine}{} \qquad (4)$$

for which an equilibrium constant may be defined as:

$$K* = ([Al_2O_3]_{int} - [Al_2O_3]_o)/\left(\left(a_{Al_2O_3}\right)^{1/2}\left(a_{SiO_2}\right)^{3/4} \right) \qquad (5)$$

where $[Al_2O_3]_{int}$ is the observed interface concentration obtained from fitting the diffusion profiles (in ppm), and $[Al_2O_3]_o$ is the original Al_2O_3 concentration in the forsterite crystal, taken here as 30 ppm. This original Al_2O_3 is assumed to be substituting by the conventional coupled mechanism (i.e., as $MgAl_2O_4$) and to be immobile on the timescales of the experiments; it should therefore to be subtracted out to reveal the interface concentration of Al_2O_3 corresponding to the fast-diffusing OSCV substitution mechanism. We also assume that the activity of the $Al_{4/3}^{3+}vac_{2/3}SiO_4$ component to the power of 3/4 is proportional to the concentration of Al in olivine, which is required by the observation that Henry's law is followed for the olivine/melt partitioning relations of other 3+ cations thought to substitute in olivine by the same OSCV mechanism, namely Sc^{3+} and REE^{3+} (Evans et al. 2008). The equilibrium constant defined in Eq. (5) is denoted $K*$, as the standard states of SiO_2 and Al_2O_3 are the conventional ones of quartz and corundum at the temperature of interest, that for Al in olivine is the component at infinite dilution, in units of ppm of Al_2O_3. $K*$ therefore has units of ppm, and implicitly includes the Henry's law activity

coefficient of Al_2O_3 in olivine substituting by the OSVC mechanism. Values of $log_{10} K*$ calculated from Tables 2 and 4 are plotted against 1/T in Fig. 5b, from which it may be seen that the different buffer assemblages give consistent values regardless of whether they have melted or not. Note also the steep slope in this plot, reflecting the large increase in interface concentrations with temperature.

The diffusion coefficients were fitted to the Arrhenius equation:

$$log_{10}D = log_{10}D_o - E_a/2.303RT \qquad (6)$$

The following relationships were obtained for the three buffers that were investigated over a reasonable interval of temperature (including their supersolidus equivalents), for diffusion along [100] (Fig. 6).

$$fo + en + crd : log_{10}D = -1.52 \pm 1.41 - (360.2 \pm 42.9)/ \\ 2.303RT \ \chi_v^2 = 3.6 \qquad (7)$$

$$fo + crd + sp : log_{10}D = -1.63 \pm 1.72 - (366.9 \pm 42.9)/ \\ 2.303RT \ \chi_v^2 = 0.9 \qquad (8)$$

$$fo + sp + per : log_{10}D = -6.57 \pm 1.27 - (303.8 \pm 38.5)/ \\ 2.303RT \ \chi_v^2 = 0.8 \qquad (9)$$

The data were weighted using either the standard deviations in $log_{10}D$ given in Table 4 or ±0.15, whichever is
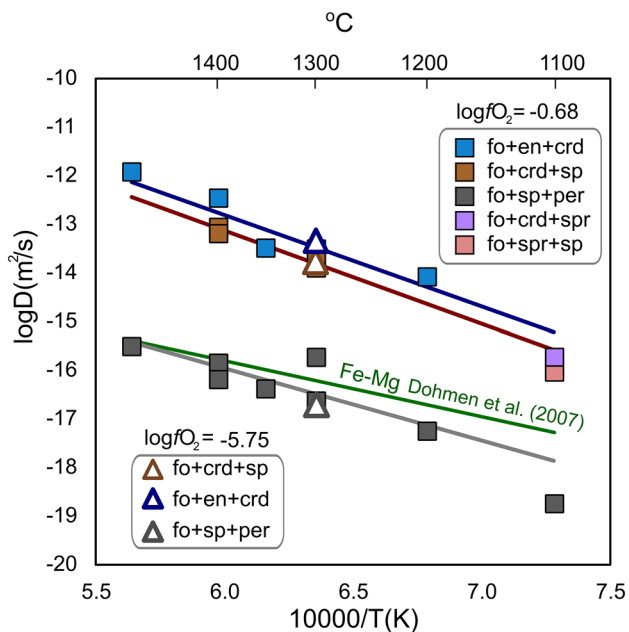
Fig. 6 Temperature dependence (Arrhenius plots) for the fast mechanism of Al diffusion in forsterite, compared to Fe–Mg inter-diffusion from Dohmen et al. (2007) and Dohmen and Chakraborty (2007). The equation $\log[D_{FeMg}(m^2/s)] = -8.91 - (220,000 + (P - 10^5) \times 7 \times 10^{-6})/2.303RT + 3(X_{Fe} - 0.1)$ was used to fit the data, with $P = 101,325$ Pa and $X_{Fe} = 0$

greater, to allow for systematic uncertainties including temperature control and imprecision in locating the position of the diffusion interface, as discussed in Zhukova et al. (2014). The values of E_a are in kJ/mol, and χ_v^2 is the reduced Chi squared for the regression. We omitted the datum at 1300 °C, run for 600 h and buffered by fo + sp + per, as it is anomalous relative to an almost identical experiment run for 672 h, 312 h and the other experiments in this series (Fig. 6).

The difference in diffusion coefficients between the low a_{SiO2} experiments (fo + sp + per) and the high a_{SiO2} experiments (fo + en + crd and fo + crd + sp) is approximately three orders of magnitude. The activation energies (E_a) for the two high a_{SiO2} assemblages are larger than for the low a_{SiO2} assemblage of fo + sp + per, implying different diffusion mechanisms and/or point-defect structures. There is no perceptible change in slope across the solidi of the two high a_{SiO2} buffering assemblages, an important observation as it discounts the possibility that diffusion rates are influenced by the presence of melt in these assemblages.

San Carlos olivine

The experiment on San Carlos olivine was conducted at a temperature of 1300 °C and $\log fO_2 = -5.8$, corresponding to 1.5 log units above the extrapolation to 1300 °C

of the quartz-fayalite-magnetite buffer curve of O'Neill (1987). An attempt was made to study the same four buffering assemblages that were used in the forsterite experiments. Olivine crystals appeared to be homogeneous in Mg and Fe after the experiments within the standard deviation. Mg# measured by EMPA in different crystals was 0.91 (2.5% RSD). Two of the assemblages containing (Mg, Fe^{2+})Al_2O_4 spinel (sco + crd + sp and sco + mw + sp where mw is magnesiowüstite) gave extremely noisy profiles as the interface was approached. We interpret this to be due to precipitation of submicroscopic spinel caused by the natural concentrations of Cr^{3+} and Fe^{3+} in the San Carlos olivine, which would stabilize spinel at lower Al concentrations in the olivine than that at the interface due to forming (Mg, Fe^{2+})(Al, Cr^{3+}, Fe^{3+})$_2O_4$ solid solutions. Hence spinel precipitation would occur unless there was some kinetic barrier to its nucleation. The lack of any such barrier is indicated by the common occurrence of picotite exsolutions in olivines, especially olivine phenocrysts in island-arc basalts. The assemblage without spinel (sco + opx + crd) gave profiles with considerably less noise but still had more noise compared to experiments with forsterite, which made fixing the position of the interface difficult. Being undersaturated in (Mg, Fe^{2+})Al_2O_4 spinel in the buffering assemblage made spinel precipitation less likely in this experiment. Our estimate of the interface concentration is 430 ppm Al_2O_3, with an uncertainty estimated at approximately ±50 ppm. The initial concentration was 230 ppm, giving an increase in Al_2O_3 of about 200 ppm but with a large uncertainty.

Despite containing spinel in the buffering assemblage, the crystal buffered by sco + crd + sp produced diffusion profiles of similar quality to the experiments with forsterite, with an interface concentration of 430 ppm Al_2O_3, which is twice that in experiments on forsterite at the same temperature and three-phase buffering assemblage of 215–230 ppm (Table 5). It is nevertheless distinctly below the expected equilibrium concentration of ~1100 ppm Al_2O_3 at 1300 °C from Al-in-olivine geothermometry (Wan et al. 2008; Coogan et al. 2014). However, the initial concentration of Al_2O_3 in this crystal of San Carlos olivine was 230 ppm, substantially more than the 30 ppm in the synthetic forsterite, hence the augmentation of Al at the interfaces ([Al_2O_3]$_{int}$ − [Al_2O_3]$_o$), representing the concentration of Al added by the diffusion experiment, is similar. The diffusivity of Al was approximately an order of magnitude slower than in forsterite at equilibrium with the fo + crd + sp buffer at the same temperature and oxygen fugacity. Part of this may be an orientation effect, as the orientation of this crystal was not determined, although the [001] orientation of the fosterite diffusion experiments is usually not the fastest, being, for most elements, intermediate between [100] and

[010], such that a log-unit difference seems excessive (Spandler and O'Neill 2010).

As observed by Spandler and O'Neill (2010), Zn was lost from all four crystals of San Carlos olivine during the annealing experiments, producing good diffusion profiles, with concentrations that ranged from ~60 ppm in the original crystals to ~10 ppm at the interface. These profiles were also well fit by the error function (Eq. 3), and gave diffusion coefficients resolvably different from those for Al diffusing in San Carlos olivine at 1300 °C (Table 4).

Despite the unresolved issues, this experiment demonstrates that the fast diffusion of Al occurs in natural olivines, and is not just some artifact of Czochralski-grown synthetic forsterite.
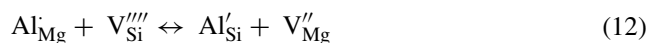
Discussion

The ways that Al may be incorporated into olivine have been discussed previously by Agee and Walker (1990), Beattie (1994), Colson et al. (1989), Evans et al. (2008), Grant and Wood (2010), Milman-Barris et al. (2008), Nielsen et al. (1992), Taura et al. (1998), Wan et al. (2008), Zhang and Wright (2010) and Coogan et al. (2014). Our results indicate that although the coupled substitution producing the component $MgAl_2O_4$, and expressed in Kröger–Vink notation as:

$$Mg^x_{Mg} + Si^x_{Si} \leftrightarrow Al^{\cdot}_{Mg} + Al'_{Si} \tag{10}$$

is likely the dominant one in the simple system MgO–Al_2O_3–SiO_2 at equilibrium, as has been widely assumed (e.g., Coogan et al. 2014), a minor proportion of Al also substitutes by the OSVC mechanism:

$$3Mg^x_{Mg} \leftrightarrow 2Al^{\cdot}_{Mg} + V''_{Mg} \tag{11}$$

These two substitution mechanisms appear each to be tied to its own diffusion mechanism. The $MgAl_2O_4$ substitution is associated with slow diffusion, presumably rate-limited by the diffusivity of Si, because this substitution requires that half the Al replaces Si on tetrahedral sites. It occurs so slowly that it is not seen under our experimental conditions with the spatial resolution achievable by our analytical method. In contrast, the OSVC substitution (producing the component $Al^{3+}_{4/3}vac_{2/3}SiO_4$) is associated with diffusion that is many orders-of-magnitude faster, presumably because it involves Al occupying only octahedral sites. The separation of the two substitution mechanisms by the two diffusion mechanisms may seem surprising if it were supposed that Al could diffuse rapidly along an octahedral-site pathway, and then exchange with a tetrahedral-site vacancy:
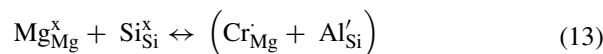
$$Al^{\cdot}_{Mg} + V''''_{Si} \leftrightarrow Al'_{Si} + V''_{Mg} \tag{12}$$

That this does not happen may indicate that the concentrations of tetrahedral vacancies (V''''_{Si}) are much less than the relevant concentrations of Al.

Diffusion of Al in our experiments is many orders of magnitude faster than that expected for tetrahedral-site diffusion, based on the diffusivity of Si (e.g., Fei et al. 2012 and references therein). At high a_{SiO_2} it is approximately 1.5 orders of magnitude faster than Fe–Mg interdiffusion and REE diffusion in olivine at 1300 °C along [100] (Spandler and O'Neill 2010). This fast diffusivity may be related to the creation of octahedral-site vacancies by the proposed substitution mechanism. In contrast, at low a_{SiO_2} (hence high a_{MgO}), diffusivities are three orders of magnitude slower, a rather greater effect than found for the diffusivities of Ni^{2+} and Co^{2+} (Zhukova et al. 2014) or Zr^{4+} and Hf^{4+} (Jollands et al. 2014).

Although the experiments reported in this study address the simple system MgO–Al_2O_3–SiO_2, the experiment on the San Carlos olivine shows that fast-diffusing mechanism also applies to natural olivines. Therefore, it is likely that other substitution mechanisms of Al become important in natural, compositionally complex olivines, including:

a. tetrahedral Al^{3+} charge balanced by some other aliovalent cations such as Fe^{+3} or Cr^{+3} in octahedral sites (e.g., Bershov et al. 1983), either coupled or uncoupled by short-range order, e.g.:

$$Mg^x_{Mg} + Si^x_{Si} \leftrightarrow \left(Cr^{\cdot}_{Mg} + Al'_{Si} \right) \tag{13}$$

b. Al^{3+} in octahedral sites charge balanced by monovalent cations such as Li^{+1} or Na^{+1} also in octahedral sites, again with or without short-range order:

$$2Mg^x_{Mg} \leftrightarrow Al^{\cdot}_{Mg} + M'_{Mg} \tag{14}$$
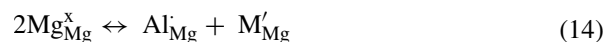
c. octahedral Al^{3+} associated with H substitution forming OH^- anions, as found by FTIR spectroscopy (e.g., Berry et al. 2005).

If the principle deduced from this study of fast diffusion of octahedral Al but very slow diffusion of tetrahedral Al is maintained for these compositionally complex substitutions, then it would be expected that Al substituting by mechanism (a) would be immobile whereas Al associated with mechanisms (b) or (c) would diffuse relatively rapidly. Fast octahedral-site diffusion might be expected to allow partial diffusive equilibration of Al zoning, blurring such zoning compared to that of phosphorus, assuming that P

occurs only on the ultra-slow diffusiving tetrahedral sites of olivine.

Evans et al. (2008) observed that the concentration of Al in olivine was approximately proportional to the square root of its concentration in coexisting silicate melt, indicating that the dominant substitution mechanism (the $MgAl_2O_4$ substitution mechanism) occurred by a coupled substitution between octahedral and tetrahedral Al, with a high degree of short-range order. By contrast, we expect that Al in olivine substituting by the OSVC mechanism would be proportional to its concentration in the melt, rather than the square root of its concentration, because this proportionality (corresponding to Henry's law) is observed for large R^{3+} cations, like Sc and the REE, that also substitute in olivine by the OSVC mechanism (Beattie, 1994; Evans et al. 2008). In other words, the OSVC mechanism has relatively higher configurational entropy than the $MgAl_2O_4$-like mechanism. Consequently, the OSVC mechanism should become relatively more important at higher temperatures than the 1300 °C of this study, and also at alumina activities lower than those studied here. The effect of pressure is unknown.

Conclusions

Although the possibility of multiple substitution mechanisms for a trace element in a mineral has seemed plausible on crystal-chemical grounds, this phenomenon has rarely been documented experimentally. An important exception is the substitution of H in nominally anhydrous minerals like olivine (e.g., Berry et al. 2005, 2007), where the sensitivity of the substitution mechanism to IR spectroscopy enabled the multiplicity of mechanisms to be identified. Here we use a different experimental approach to provide evidence for an essentially similar phenomenon. This study also highlights the important consequences of multiple substitution mechanisms for trace element geochemistry. For example, multiple substitution mechanisms add complexity to the compositional dependence of partition coefficients, including their "stoichiometric control" (e.g., O'Neill and Eggins 2002), as demonstrated here by the different dependence of the OSVC mechanism on a_{SiO2} compared to the dominant $MgAl_2O_4$-type substitution in olivine. This study also provides another example of different substitution mechanisms being associated with enormously different transport properties, which may be a common phenomenon in the complex natural crystals. In olivine, for example, different diffusion mechanisms have now been observed for Li (Dohmen et al. 2010), H (e.g., Padrón-Navarta et al. 2014 and references therein) and Ti (Jollands et al. 2016a, b).

References

Agee CB, Walker D (1990) Aluminum partitioning between olivine and ultrabasic silicate liquid to 6-Gpa. Contrib Miner Petrol 105:243–254

Batanova VG, Sobolev AV, Kuzmin DV (2015) Trace element analysis of olivine: high precision analytical method for JEOL JXA-8230 electron probe microanalyser. Chem Geol 419:149–157

Beattie P (1994) Systematics and energetics of trace-element partitioning between olivine and silicate melts—implications for the nature of mineral melt partitioning. Chem Geol 117:57–71

Berry AJ, Hermann J, O'Neill HSC, Foran GJ (2005) Fingerprinting the water site in mantle olivine. Geology 33:869–872

Berry AJ, O'Neill HSC, Hermann J, Scott DR (2007) The infrared signature of water associated with trivalent cations in olivine. Earth Planet Sci Lett 261:134–142

Bershov LV, Gaite JM, Hafner SS, Rager H (1983) Electron-paramagnetic resonance and endor studies of Cr^{3+}–Al^{3+} pairsin forsterite. Phys Chem Miner 9:95–101

Chakraborty S (2010) Diffusion coefficients in olivine, wadsleyite and ringwoodite. Rev Miner Geochem 72:603–639

Colson RO, Mckay GA, Taylor LA (1989) Charge balancing of trivalent trace-elements in elivine and low-Ca pyroxene—a test using experimental partitioning data. Geochim Cosmos Acta 53:643–648

Connolly JAD, Petrini K (2002) An automated strategy for calculation of phase diagram sections and retrieval of rock properties as a function of physical conditions. J Metamorph Geol 20:697–708

Coogan LA, Saunders AD, Wilson RN (2014) Aluminum-in-olivine thermometry of primitive basalts: evidence of an anomalously hot mantle source for large igneous provinces. Chem Geol 368:1–10

Dohmen R, Chakraborty S (2007) Fe–Mg diffusion in olivine II: point defect chemistry, change of diffusion mechanisms and a model for calculation of diffusion coefficients in natural olivine. Phys Chem Miner 34:597–598

Dohmen R, Becker HW, Chakraborty S (2007) Fe-Mg diffusion in olivine I: experimental determination between 700 and 1,200 degrees C as a function of composition, crystal orientation and oxygen fugacity. Phys Chem Miner 34:389–407

Dohmen R, Kasemann SA, Coogan L, Chakraborty S (2010) Diffusion of Li in olivine. Part I: Experimental observations and a multi species diffusion model. Geochim Cosmos Acta 74(1):274–292

Evans TM, O'Neill HSC, Tuff J (2008) The influence of melt composition on the partitioning of REEs, Y, Sc, Zr and Al between forsterite and melt in the system CMAS. Geochim Cosmos Acta 72:5708–5721

Fei H, Hegoda C, Yamazaki D, Wiedenbeck M, Yurimoto H, Shcheka S, Katsura T (2012) High silicon self-diffusion coefficient in dry forsterite. Earth Planet Sci Lett 345:95–103

Foley SF, Jacob DE, O'Neill HSC (2011) Trace element variations in olivine phenocrysts from Ugandan potassic rocks as clues to the chemical characteristics of parental magmas. Contrib Miner Petrol 162:1–20

Grant KJ, Wood BJ (2010) Experimental study of the incorporation of Li, Sc, Al and other trace elements into olivine. Geochim Cosmos Acta 74:2412–2428

Heinonen JS, Jennings ES, Riley TR (2015) Crystallisation temperatures of the most Mg-rich magmas of the Karoo LIP on the basis of Al-in-olivine thermometry. Chem Geol 411:26–35

Holland TJB, Powell R (2011) An improved and extended internally consistent thermodynamic dataset for phases of petrological

interest, involving a new equation of state for solids. J Metamorph Geol 29:333–383

Ingrin J, Kovács I, Deloule E, Balan E, Blanchard M, Kohn SC, Hermann J (2014) Identification of hydrogen defects linked to boron substitution in synthetic forsterite and natural olivine. Am Miner 99(10):2138–2141

Jaoul O, Houlier B, Abel F (1983) Study of ^{18}O diffusion in magnesium orthosilicate by nuclear microanalysis. Geophys Res Lett 88:613–624

Jollands MC, O'Neill HSC, Hermann J (2014) The importance of defining chemical potentials, substitution mechanisms and solubility in trace element diffusion studies: the case of Zr and Hf in olivine. Contrib Miner Petrol 168:1055

Jollands MC, Burnham AD, O'Neill HSC, Hermann J, Qian Q (2016a) Beryllium diffusion in olivine: a new tool to investigate timescales of magmatic processes. Earth Planet Sci Lett 450:71–82

Jollands MC, Hermann J, O'Neill HSC, Spandler C, Padrón-Navarta JA (2016b) Diffusion of Ti and some divalent cations in olivine as a function of temperature, oxygen fugacity, chemical potentials and crystal orientation. J Petrol 57(10):1983–2010

Mallmann G, O'Neill HSC, Klemme S (2009) Heterogeneous distribution of phosphorus in olivine from otherwise well-equilibrated spinel peridotite xenoliths and its implications for the mantle geochemistry of lithium. Contrib Miner Petrol 158:485–504

Mao H, Fabrichnaya O, Selleby M, Sundman B (2005) Thermodynamic assessment of the $MgO–Al_2O_3–SiO_2$ system. J Mater Res 20:975–986

Martrosov VN, Matrosova TA, Kupchenko MI, Pestryakov EV, Pavlovskij LK (2002) Growth of activated forsterite crystals. Poverkhnost Rentgenovskie sinkhronnye i nejtronnye issledovaniya 5:30–34

McKibbin SJ, O'Neill HC, Mallmann G, Halfpenny A (2013) LA–ICP–MS mapping of olivine from the Brahin and Brenham meteorites: complex elemental distributions in the pallasite olivine precursor. Geochim Cosmos Acta 119:1–17

Milman-Barris MS, Beckett JR, Baker MB, Hofmann AE, Morgan Z, Crowley MR, Vielzeuf D, Stolper E (2008) Zoning of phosphorus in igneous olivine. Contrib Miner Petrol 155:739–765

Nielsen RL, Gallahan WE, Newberger F (1992) Experimentally determined mineral-melt partition-coefficients for Sc, Y and Ree for olivine, ortho-pyroxene, pigeonite, magnetite and ilmenite. Contrib Miner Petrol 110:488–499

O'Neill HSC (1987) Quartz-fayalite-iron and quartz-fayalite-magnetite equilibria and the free energy of formation of fayalite (Fe_2SiO_4) and magnetite (Fe_3O_4). Am Miner 72:67–75

O'Neill HSC, Eggins SM (2002) The effect of melt composition on trace element partitioning: an experimental investigation of the activity coefficients of FeO, NiO, CoO, MoO_2 and MoO_3 in silicate melts. Chem Geol 186(1):151–181

Qian Q, O'Neill HSC, Hermann J (2010) Comparative diffusion coefficients of major and trace elements in olivine at similar to 950 degrees C from a xenocryst included in dioritic magma. Geology 38:331–334

Spandler C, O'Neill HSC (2010) Diffusion and partition coefficients of minor and trace elements in San Carlos olivine at 1,300 degrees C with some geochemical implications. Contrib Miner Petrol 159:791–818

Spandler C, O'Neill HSC, Kamenetsky VS (2007) Survival times of anomalous melt inclusions from element diffusion in olivine and chromite. Nature 447:303–306

Spice H, Sanloup C, Cochain B, de Grouchy C, Kono Y (2015) Viscosity of liquid fayalite up to 9 GPa. Geochim Cosmos Acta 148:219–227

Taura H, Yurimoto H, Kurita K, Sueno S (1998) Pressure dependence on partition coefficients for trace elements between olivine and the coexisting melts. Phys Chem Miner 25:469–484

Tollan PME, O'Neill HSC, Hermann J, Benedictus A, Arculus RJ (2015) Frozen melt-rock reaction in a peridotite xenolith from sub-arc mantle recorded by diffusion of trace elements and water in olivine. Earth Planet Sci Lett 422:169–181

Tuff J, O'Neill HSC (2010) The effect of sulfur on the partitioning of Ni and other first-row transition elements between olivine and silicate melt. Geochim Cosmos Acta 74:6180–6205

Wan ZH, Coogan LA, Canil D (2008) Experimental calibration of aluminum partitioning between olivine and spinel as a geothermometer. Am Miner 93:1142–1147

Watson EB, Cherniak DJ, Holycross ME (2015) Diffusion of phosphorus in olivine and molten basalt. Am Miner 100:2053–2065

Zhang FW, Wright K (2010) Coupled (H^+, M^{3+}) substitutions in forsterite. Geochim Cosmos Acta 74:5958–5965

Zhukova IA, O'Neill HSC, Campbell IH, Kilburn MR (2014) The effect of silica activity on the diffusion of Ni and Co in olivine. Contrib Miner Petrol 168:1–15